Photoelectron microscopy: VPPEM

A forward view position paper.

Raymond Browning,

R. Browning Consultants. February 2015

Abstract

We propose that this is an appropriate time to combine high energy X-ray photoelectron spectroscopies with low energy photoelectron microscopies. There are several new technology opportunities that can be exploited, and there is also a technology driver in the need to analyze mesoscale engineered materials.

In this discussion we shall make a case for a synthesis between four developments. The first development is proof of principle experiments with HAXPES microscopy, the second is the development of a new imaging photoelectron microscopes, the third is new methods in image processing, and the fourth is the development of beamlines with a wide photon energy range at third generation synchrotrons. These developments naturally fit together, and we believe they will form a vital part of the tool set for materials analysis at the mesoscale.

The actual pieces are in place for his new synthesis, including the commissioning of NSLS II at Brookhaven Laboratory, and a new photoelectron microscopy technique, VPPEM.

Introduction

X-ray photoelectron spectroscopies are important material analysis techniques in a wide field of technology areas from semiconductor device to catalysis. Photoelectron spectroscopies give elemental compositions, chemical state, local atomic coordination, semiconductor band structure, magnetic properties, and other details of materials structure, and makeup. The field of applications is still broadening with the rapid development of specific techniques enabled by the availability of extended spectral range photons from the third generation of synchrotron light sources. In particular high energy x-ray photoelectron spectroscopy HAXPES is rapidly developing into a key technology for mesoscale materials analysis. The main feature of HAXPES for these applications is the longer mean free path (MFP) of the photoelectrons at high energies. The longer electron MFP (over 100 nm) is a tool for comparison of the surface, and bulk of a sample so that a model of the near surface elemental, and chemical distributions can be made, or in the case of catalysis, information can be extracted through a gas surrounding the catalyst. The long MFP also means that HAXPES is less to do with surface science technique but more to do with real world material analysis, for example, diffusion across buried interfaces in semiconductor devices. The next instrumental challenge is taking development of the HAXPES technique beyond high energy photoelectron spectroscopy to high energy photoelectron microscopy. Microscopy has only played a minor role in the development of HAXPES, although excellent proof of principle results have been obtained, and it can be seen that instrumental methods are leading towards some exciting developments. These instrumental developments come at an opportune time as we have a technology driver. There is a pressing need for chemical state analysis on the mesoscale [1] for which HAXPES microscopy as an active, and expanding field could make a significant contribution.

At the National Synchrotron Light Source (NSLS) at the DOE Brookhaven National Laboratory, we have been developing a new class of photoelectron microscope, the vector potential photoelectron microscope (VPPEM). In this white paper I will try to demonstrate why I think HAPEXES microscopy is about to undergo rapid development, and how VPPEM fits in to the general picture of real world mesoscale materials analysis.

The slower development of HAXPES microscopy, is due both to physical factors, and also the operational basis of the most popular types of photoelectron microscope. The main physical factor is simply that the signal from HAXPES is much lower for the same photon flux than at lower energies because of the reduced photoionization cross section at higher energies. By its nature, microscopy requires much more signal than spectroscopy so the loss of intensity in the characteristic electron signal is a serious penalty. The second issue is that the main class of high spatial resolution photoelectron microscope preferentially uses low energy electrons for imaging. The photoelectron emission microscope (PEEM) class of instruments are derived from the low energy electron microscope (LEEM) [2, 3] which uses a strongly accelerating cathode lens with the sample as

the cathode. While the recent development of the vector potential photoelectron microscope (VPPEM) [4, 5] does not use a cathode lens, it also requires a strong signal, and the highest spatial resolutions are also achieved using low energy electrons.

Other approaches to photoelectron microscopy include the different variants of the scanning X-ray microprobe. Of the two main approaches to forming the scanning probe, the focusing mirror systems seem intuitively more likely to have value for HAXPES imaging [6]. The zone plate approach while not confined to lower energy x-rays does have other technical and design issues to overcome, such as probe formation over a wide energy range [7]. However, the physical limitation still remains that microscopy requires a large signal. It is for this reason most high energy microprobe imaging uses signal channels such as x-ray fluorescence, Bragg diffraction, or x-ray absorption which have large signal strengths in comparison to HAXPES photoelectrons [8]. However, we shall argue below that the integration of different signal channels into HAXPES imaging is a route to overcoming many of the difficulties of HAXPES imaging, and leads to new opportunities for photoelectron microcopy. For this reason the low energy microscope looks most interesting as a basis for further developments.

For HAXPES spectroscopy the photoelectron directly emitted from a core level, the XPS signal or the photo peak, is typically the information channel of interest. The information depth for this signal has become well understood [9, 10], and using both the change in MFP with energy, and change in detection angle gives the structure of buried layers. This direct high energy signal also includes shakeup features, recoil effects, interatomic transitions, and other rich details of composition and structure. However, for microscopy these additional signals will be second order, and much weaker. Other signals created by the high energy photons such as x-ray absorption spectra (XAS) [11] and its derivatives, near edge x-ray absorption fine structure (NEXAFS) [12] and extended x-ray absorption fine structure (EXAFS) [13] are more accessible for imaging as they have a significant low energy partial yield (PAY). However, using a low energy signal such as PAY NEXAFS brings up the question of what then is the information depth.

In summary, there are several information channels which we could consider to be HAXPES which include the direct photo peak and the photoelectron yield response to x-ray absorption. While there are several ways to create the image we shall concentrate on the extension of the low energy microscopies to high energies, neglecting the contributions from scanning probe systems.

HAXPES microscopy, HAXPEEM

At present, the number of examples of photoelectron microscopy using high energy photons and the directly emitted HAXPES photo peak as an imaging channel are limited. While several groups have used PEEM with high energy photons as the excitation, they image with low energy electron signals [14- 18], this is not the same thing as using the long MFP of the photoelectrons directly. However, we do have what might be considered the holotype experiment for HAXPES in a PEEM [19, 20]. This experiment was performed at PETRA III on an undulator beam line, and gives us a clear indication of the orders of magnitude to be expected in spatial resolution, photon flux, and image collection times.

Basic PEEM is naturally a low energy imaging technique, 0-50 eV. The limit to using higher energies is the decrease in collection angle needed to make a high resolution image with energy filtering in an analyzer. The solid angle for a PEEM imaging several keV electrons is reduced to the order of 0.1%. Taken with the decrease in sensitivity of HAXPES this requires a very bright photon source to achieve submicron spatial resolution. Even so, imaging at PETRA III took an extended exposure time of 120 minutes. FIG. 1 shows the results from a Au/Si calibration sample using 4294 eV Au photoelectrons [19, 20].

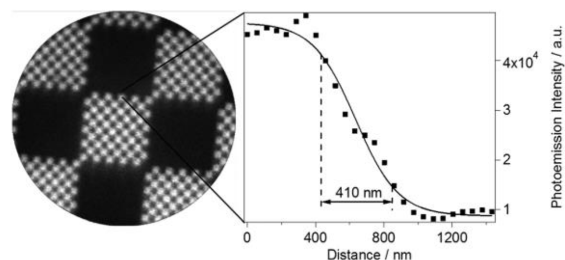

FIG. 1. Au/Si calibration sample imaged on the Au 3d5/2 photoemission line at a kinetic energy of 4294 eV (left). Line scan across a square edge and 16/84% profile fit (right). Refs [19, 20]

The line scan on the left of FIG. 1 shows better than 500nm spatial resolution across an edge. Depth profile data can also be obtained. FIG. 2 shows results from Au islands on $SrTiO_3$ using 6.5keV photons, and the Sr $2p_{3/2}$ transition [19]. From the intensity loss, a MFP at 4560eV of 8.5nm was estimated. The departure from the calculated value of 4.4nm [21] is argued to be due to surface roughness. What perhaps is more interesting, is the shift in the buried layer Sr peak position by 0.4eV to a lower binding energy. As this signal will more strongly represent the Au/$SrTiO_3$ interface, it shows that the interface states differ from the bulk, and this can be imaged.

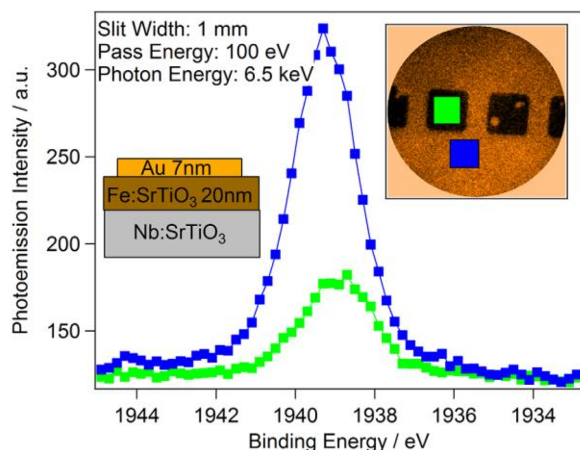

FIG. 2. Selected area hard x-ray photoemission spectra from Al/$SrTiO_3$. Inset top right: definition of regions of interest. Inset left: sample layer composition. Refs [19, 20]

The advantage of a PEEM instrument for this experiment is that both very low energy imaging, and HAXPES imaging can be performed on the same sample area. By switching focusing conditions, and turning on a different light source, in this experiment a mercury discharge lamp, a very wide range photoelectron energies can be collected.

The PEEM used for the results of Figs 1 and 2 was operated with an accelerating electrostatic lens with 24kV extraction voltage. An electrostatic electron lens operated under these conditions is a very good lens, having both low spherical and chromatic aberrations. Although, with high energy electrons it is a low power lens with only a 6.6:1 accelerating ratio. This means that the solid angle of acceptance must be reduced to give a reasonable spatial resolution, in this case implying a 0.15% transmission. While this is still a relatively high sensitivity the low cross section of the HAXPES makes for a lengthy collection time of 2 hours per image. The authors did not estimate the beam flux density they used but we might expect of the order of 10^8 photons/sec/μ^2 from the P09 beamline they used. In comparison, an increase of at least two orders of magnitude might be expected from current beamline developments, and a corresponding improvement in the spatial resolution down to 50 nm. Although a factor 10 decrease in the exposure time taken with a factor 3 increase in spatial resolution is more likely given that sample position stability might become an issue below 100 nm. The high flux does impose limitations on the types of samples that can be imaged, but the typical high flux problem of space charge broadening at the backplane crossover is not an issue for high energy imaging [22]. Note, we also expect also a change in magnification going from low energy operation to high energy but this can be accurately compensated for.

As a comparison with what we could call true HAXPES imaging, an alternative is to use high energy photons but image with low energy electrons. The low energy information channel gives a much stronger signal, while still giving an enhanced probing depth over soft x-ray operation [16], and reasonable spatial resolution at the solid surface. This enhanced probing depth is due to a longer MFP of the higher energy Auger electrons. The energy loss mechanisms being largely plasmon losses which have low lateral momentum loss but lead to an increase in secondary electrons at the surface [17]. Thus high energy x-ray photons combined with low energy PAY NEXAFS will have a similar probing depth to HAXPES, and with a spatial resolution that will depend on the information depth.

Images with good contrast and signal-to-noise have been be obtained by imaging the K edge of Co (7.71 keV) [17]. Also 200 nm spatial resolution was obtained using x-ray magnetic circular dichroism (XMDC) even with Pt L_2 (13.27keV) in CoCrPt films [17]. This last result with only 10^7 photons/sec/μ^2 (SPring8 BL39XU) [23]. Note that these low energy results are from a direct imaging PEEM with no energy analysis, so that true HAXPES imaging would not have been possible. But they demonstrate that extension of PEEM to higher photon energies is a natural development, and important results can be obtained with current instruments. The SPring8 BL39XU has now been converted to a hard x-ray nanospectroscopy (XAFS and XMCD) station with a

beam size of 100 nm and a flux density of $6x10^{11}$ photons/sec/μ^2 using Kirkpatrick-Baez mirrors [7].

Clearly, from the PETRA results [19, 20] an extension to a true HAXPES PEEM (HAXPEEM) with a few 10's of nanometer resolution is very possible with a higher beam brightness. But much more can be achieved. The HAXPEEM is essentially looking at a colored world through a monochrometer. In principle, the HAXPEEM has access to a wide range of photon energies, and can detect electrons with energies from zero up to over 10keV. In fact, the same instrument used for HAXPEEM was also used for imaging the checkerboard of FIG. 1 with the low energy Si 2p and the Au $4f_{7/2}$, and with similar imaging quality [19]. This is not a trivial observation, bringing information together (data fusion) from across the photon, and electron detection ranges creates new information, and this has been successfully implemented in several fields from remote sensing to medical imaging [24-27]. Image processing using correlations between low energy spectral features with strong signals, and noisy high energy features can improve the effective spatial resolution of the higher energy features. Binning of hyperspectral image pixels can separate out edge effects from feature centers in complex images, and very small volumetric densities can be isolated from a matrix. Image fusion across different image types can expose subtle correlations that would be otherwise overlooked. Taken together with higher beam flux densities, hyperspectral imaging could push effective HAXPES spatial resolutions into the mid and low 10's of nanometers. For some applications the availability in the one instrument of a wide hyperspectral range might be the most important advantage of this class of microscope over the scanning microprobe. Also, in some circumstances the very low energy and high energy electron MFP's may be similar [28]. This makes data fusion much more direct, and the combination of information from the two ends of the spectrum very powerful. Taken with the fact that both PEEM and VPPEM have higher spatial resolution, and much stronger signals at lower energies, there seems to be a case for combining HAXPES imaging with low electron energy x-ray photoelectron spectroscopic imaging (LEEXPES), and with the extended probing depth of core edge yelds using high energy photons.

Low Energy Electron Mean Free Paths

There is sufficient knowledge about low energy electron MFP's so that we can start to see how this region of the spectrum might be used in photoelectron microscopy. Unlike high energy MFP's where universal curves [9, 10] give a good guide for energies above 100 eV, for low energies, experimental data seems to be the most reliable source. There are large differences in low energy MFP's depending on the details of the electronic structure near the Fermi level. It seems that free electron theory can give trends at low energies [29, 30], but for calculations to be useful they must take the band structure of the material into account [31]. For example, the electron MFP for ytterbium 5-10eV (above Fermi level) is 1-2 nm [32], while for aluminum the MFP is 5-10 nm [33]. A big difference between ytterbium and aluminum is that ytterbium has a loss channel close to the Fermi level in the core 4f transitions [34].

The experimental data we have on low energy MFP's comes from a variety of sources, these include ultra violet photoemission [35], ballistic electron spectroscopy [36], and energy loss spectroscopies in solids and gasses [37-41]. While much of this data is somewhat isolated at present, there is no real impediment to collecting it together for use with microscopy. Although, putting the data together does not give the universal curves of higher energies, it does tell us that imaging of electrons within a few eV of the Fermi level in solids, and between 0.5-2 eV in gases gives us MFP's that are often comparable to those in the 2-10 keV HAXPES range. Further, these MFP's scale in a useful way with energy so that they can in principle be used for depth profiling as with HAXPES spectroscopy. Significant synergies could exist between data from high accuracy HAXPES depth profiles, and high spatial resolution depth estimates from LEEXPES.

Low Energy Photoelectron Signal Sources

The information in low energy electron spectromicroscopy images can come from a number of signal sources. If we add this to high energy image data it becomes very complex. Some of this information we may see as useful, other information as noise, and an impediment to a simple measurement of elemental spatial distributions. Some of the information we want such as chemical

shifts may make image registration across a wide data range very challenging, but as we will see below the strong signal can be used to make very detailed, and informative images.

The LEEXPES signal, besides having the elemental/chemical content, may be sensitive to differential surface charging, surface topography, magnetic substrate effects, or sample bias. In particular the spatial resolution may be dependent on the surface topography as is the case for cathode lens-based photo emission electron microscopy (PEEM) [42]. Although, the VPPEM image contrast is less sensitive to many of these effects. If the illumination is not normal to the surface there will also be some illumination, and emission shadowing on rough surfaces. Roughness will also generate changes in the effective penetration depth of the x-rays with variations in the local angle of incidence to the sample surface normal.

In general, the LEEXPES signal will be a two dimensional spectral signal derived from both the secondary effect of x-ray absorption such as the core edge absorption yield, and also the directly emitted photoelectrons, the photo peak. This information is mixed with the other contrast effects. The two dimensions in the LEEXPES signal are photon energy, and detected electron energy. The LEEXPES signal will also consist of several spectral regions covering different core excitations. The LEEXPES signal is therefore a hyperspectral signal. When we are discussing imaging, our initial analytic emphasis is towards signal processing. The first aim is to create, and then partition an image into regions of interest using the structure of the hyperspectral signal as a guide. Introducing imaging to photoelectron spectroscopy in this way we will tend to use the concepts of signals rather than spectra. This is because the underlying photoelectron spectral information, core level excitation, chemical state, and coordinations, are mixed in with other contrast mechanisms. Therefore, we will depart somewhat from conventional spectroscopy terms to describe this emphasis.

The LEEXPES signal consists of the absorption yield signal, and the photo peak closely mixed together. Fig. 3 illustrates these sources of the LEEXPES signal in a schematic photoelectron emission energy level diagram. This illustration is particular for VPPEM which uses a biased sample to set the energy of the detected electrons, but is also relevant to the interpretation of PEEM data at very low energies where the analyzing energy is scanned and very similar results are obtained [43].

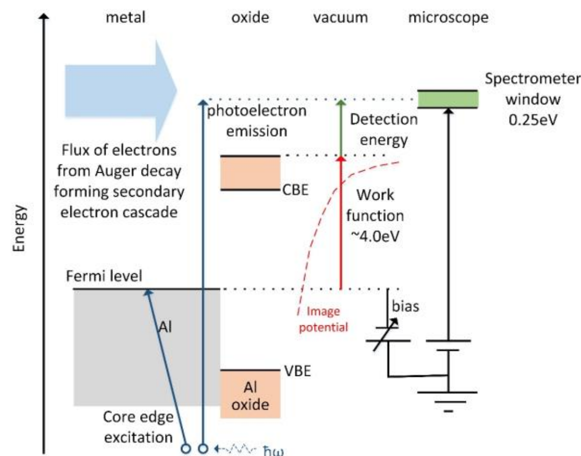

Fig. 3 Energy level diagram of the VPPEM signals from an oxidized aluminum surface, from ref [28]

In Fig. 3 the vertical direction is energy, and the horizontal direction represents distance out of the sample surface. Fig. 3 illustrates the case of an aluminum sample with an oxidized surface. The metal is on the left, and the VPPEM microscope is on the right. The sample is irradiated by x-ray photons, and if a photon, ħω, has sufficient energy it can create a core hole in the metal by removing an electron in a core state to an empty state above the Fermi level. In the case of an insulating oxide, the core electron is removed to the conduction band edge (CBE). We expect, in theory, the Fermi level in the oxide to be midway between the conduction band edge, and the top of the valence band (VBE) [44]. The photoelectron transitions in Fig. 3 are indicated by the blue vertical arrows beginning with a circle to represent the core hole remaining. Only the aluminum metal transitions have been shown. After the initial photoelectron event, the remaining core hole is filled with an electron from a higher energy level, and this initiates an Auger cascade. The Auger cascade creates a flux of inelastically scattered electrons over a wide energy range. These electrons form the secondary electron distribution when they leave the sample. The increase in the number of secondary electrons as the photon energy is swept from a low energy up across the core absorption energy is detected by the spectrometer as a PAY NEXAFS signal with a prominent feature at the core edge absorption energy.

As the photon energy is raised to several eV above the core absorption energy, the directly excited

photoelectron, the XPS electron, ejected from the aluminum metal core hole can escape the surface directly. The directly emitted electron must have a kinetic energy in the solid that is greater than the workfunction. An aluminum metal photoelectron also has to travel through the oxide overlayer without being absorbed. If the potential bias of the sample has been set so that the energy of the directly excited electron in the vacuum coincides with the energy window of the spectrometer, then the electron is detected. If the sample bias is fixed, and the photon energy is increased, the electron energy will move through the spectrometer window to produce a peak in the spectrometer signal, the photo peak. The photo peak will be superimposed on the higher energy part of the PAY NEXAFS structure because the core edge and the photo peak are only a few eV apart.

Fig. 4 shows a LEEXPES spectrum from a VPPEM. The spectrum is along the photon energy axis for a fixed detection energy of 0.5 eV. This data is from an oxidized AL surface taken from a spectral image series with photon energies from 72.5 eV to 85.0 eV in 0.5 eV steps.

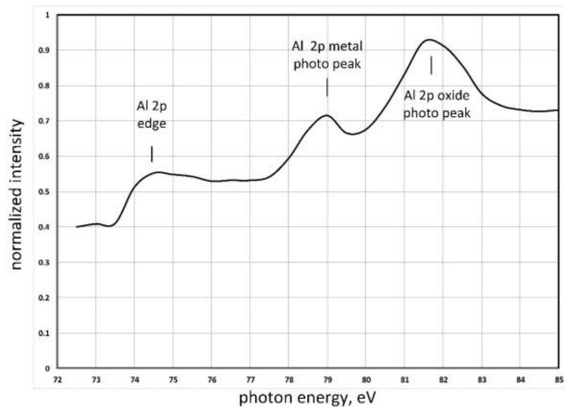

Fig. 4 VPPEM spectrum from oxidized aluminum, from ref [28]

In Fig. 4 the 2p Al metallic core absorption yield appears at 74.5 eV, and the 2p Al metallic photo peak feature would be then be expected to appear at a 4.5 eV higher energy at 79.0 eV. The extra 4.5 eV binding energy being the sum of the 4.0 eV workfunction, and 0.5 eV electron detection energy.

By changing the sample bias, the energy of the detected electrons can be changed, and he photo peaks will appear at different photon energies. Changing both the photon energy, and the detected energy, creates the two dimensional image data set. Spectra taken from an image data set from 65.0 to 95.0 eV in steps of 1.0 eV, and with detection energies 1.0, 2.0, 5.0, and 10 eV are presented in Fig. 5. The background levels have been suppressed to arrange the individual spectra in the graph.

The spectra Fig. 5a shows that there is a 2p absorption edge in the region of 74.5 eV, and there are two Al 2p photo peaks, the peak originating in the metal is indicated by the letter m, and in the oxide by the letter o. As the detected energy is changed to a higher value (by reducing the sample bias) the two Al 2p photo peaks, m and o, move together to higher photon energy, and get relatively larger.

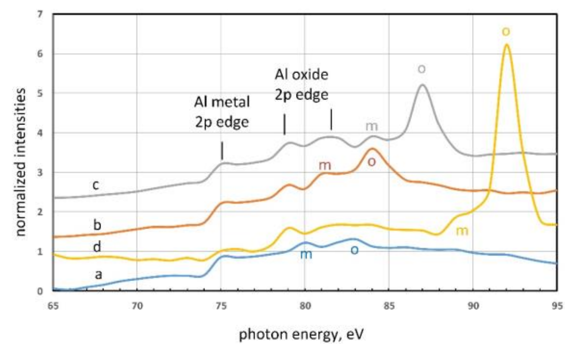

Fig. 5 Spectra from an aluminum foil with different detection energies. (a) blue, 1.0 eV, (b) brown, 2.0 eV, (c) grey 5.0 eV, (d) yellow, 10.0 eV. The spectra are shifted in the vertical direction to provide visual separation, from ref [28]

As the Al metal 2p photo peak moves higher in energy with a higher detection energy, we find that a further feature appears with a peak at 79.0 eV, just below the initial metal photo peak position at 80.0 eV, and 4.0 eV above the 2p edge. The binding energy of this new feature remains at 79.0 eV as we increase the detection energy to 10.0 eV. There also appears to be a third peak, 3.0 eV higher than the 79.0 eV peak, with the same general characteristics. These two additional features can be identified as Al 2p edges from amorphous aluminum oxide [45].

A clear feature of the spectral series in Fig. 5, is the change of relative intensity between the Al metal, and oxide photo peaks with detection energy. This change in relative intensity gives us data for depth profiling through changes in attenuation length with detection energy.

The 2p Al metal absorption edge in Fig. 5 defines the Fermi level energy for binding energies above it. This

gives us a direct measure of the energy above the Fermi energy of the photo electrons in the aluminum. From the spectral series in Fig. 5, we have the Al 2p metal photo peaks (m) at 80.0, 81.0, 84.0, and 89.0 eV, then the energies in the aluminum are 5.0, 6.0, 9.0, and 14.0 eV respectively. If the Fermi energies of the oxide, and the metal are aligned, we can expect the same energies in the oxide. The Al metal, and oxide photoelectrons pass through the same surface potential barrier, with the same final energy, and their energies in the oxide will be the same. At each of the detection energies, the surface barrier reflectivities for the metal, and oxide peaks will be the same.

To model the change in relative intensities between the Al metal, and oxide photo peaks, we used mean free paths based on simplified fits to theoretical curves in the literature [46, 47].

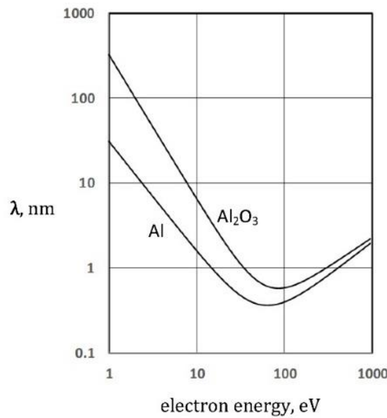

Fig. 6 Inelastic mean free path lengths for electrons in Al and Al_2O_3 from ref [28] based on refs [46, 47]

Fig. 6 shows that electron energies in the 5-15 eV range are on the rapidly changing lower part of the curves. This makes relative peak intensities very sensitive to changes in thickness in the nanometer range. For 5.0 eV, the inelastic mean free path in the metal is 4.1 nm, and for 14.0 eV it is 1.7 nm. In the oxide, the mean free paths are 22.2 nm and 4.8 nm respectively.

The MFP equations ignore elastic scattering, and are therefore not practical attenuation lengths. Above 50 eV, elastic scattering reduces the attenuation length typically by a factor 0.7-.95 [48]. However, it might be expected that elastic scattering would play a different role at lower energies, changing the shape of the low energy part of the curves in Fig. 6. This this complication is passed over, and the factor fixed at 0.8.

There are some differences to the conventional angle resolved XPS layer thickness model where the take-off angle is specified [49-51]. The VPPEM collects 2π steradians, so that angles range from 0° to 90° to the (assumed) normal. This collection angle, and the low energy of the electrons add extra details to the model. The model of the emission process uses three processes. The first process is the electron flux travelling to the solid surface. The second process is a refraction, and reflection at the surface barrier, where the critical angle limits the angular range of the model in the solid. This angular range changes with detection energy. The third process is the detection of a Lambertian distribution into the 2π solid angle collected by the VPPEM.

The results from FIG 6 are fitted by putting in a trial overlayer thickness. Fig. 7 shows the relative peak heights for the Al metal photo peaks, P_m, and the Al oxide photo peak, P_o, plotted against the energy of the electrons in the solid for an overlayer thickness of 3.5 nm [52].

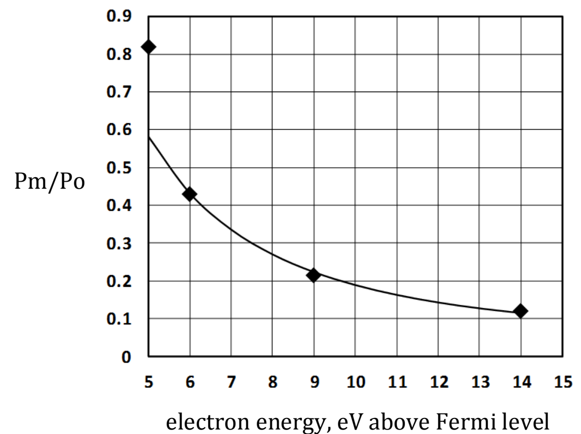

FIG. 7. Plot of relative VPPEM photo peak heights for the Al metal, P_m, and the Al oxide, P_o. Data points are from experiment, solid line from a model using a 3.5 nm oxide thickness. From ref [28].

The fit is normalized to the peak height ratio at 14.0 eV. It can be seen from Fig. 7, that the results for 14.0, 9.0, and 6.0 eV are consistent with the model. But the

fit underestimates the lower energy peak height ratio. This deviation from the model is outside what we would expect even with errors in the simple peak fitting used, clearly more work is needed to expand our understanding of the method.

Because of the many issues associated with the low energy mean free path, is unlikely that LEEXPEM based on either PEEM or VPPEM will ever reach the level of accuracy for depth profiling that is being obtained by angle resolved XPS and HAXPES. However, for VPPEM at least, the insensitivity to many common imaging artifacts gives a significant advantage in being able to get depth profile estimates from very uneven surfaces. This would include fibers, fracture surfaces, and recessed features on the nanometer scale. This suggests that low energy VPPEM would be a valuable technique to use in conjunction with data from these other methods.

From the HX-PEEM experiments [14-18] we can see that the information depth can be considerably increased by using hard x-rays, and detecting the low energy electron signal. For VPPEM this is important observation. VPPEM is a technique that will be used for real world problems in the mesoscale range. If the depth of information is restricted to the surface the technique will have less relevance.

Image Analysis in Photoelectron Microscopy

The HAXPEEM images shown in Figs 1 and 2 are only an indication of the information available from photoelectron microscopy. Much more can be achieved. Although there are no good examples of image processing with HAXPEEM, we have an example of using VPPEM in the LEEXPES mode with very low photon fluxes. With this example we can illustrate of the power of image processing in photoelectron microscopy. This example also shows us how to combine images across spectral ranges, and tells us that even with the low signal levels expected from HAXPEEM this can be finessed into giving rich image data.

In principle LEEXPES has larger signals for imaging with than HAXPES. However, the low energy signal is inherently more complex, and this in effect is adding noise to the signal. But for both the low energy and the high energy signals we can demonstrate the possibility of recovering very detailed information from noisy data by application of hyperspectral image data reduction [53].

As we have indicated, using very low energy photoelectrons for imaging raises many issues of signal interpretation. At very low energies, there are many specific surface effects to be considered in interpreting the signal. These include effects due to the surface image potential, changes in work function, local charging, and contamination. The image potential can lead to surface states that cause significant changes in transmission across the surface barrier as the take-off energy is changed. However, many of these effects will be averaged out because both the VPPEM and PEEM collect 2π steradians of the emitted electrons at low energies. Changes in workfunction across the sample will lead to a change in energy of the detected photo peak, and also the inelastic mean free path of the photoelectron. Thus, the issues of information depth, and chemical state, are factors that can be mixed together when considering image interpretation.

Imaging at low electron energies with both PEEM and VPPEM on well characterized surfaces is effective because the signals are strong, and the microscopes collect 100% of the signal. PEEM on an undulator beam line can image at video rates with 10's of nanometer spatial resolutions. This would also be expected of VPPEM which up to now has only been used on a bending magnet beamline. While PEEM is not normally used for imaging specifically at electron energies at or below 1.0 eV the direct imaging of work function changes using these energies is possible [43]. VPPEM on the other hand has the highest spatial resolution at very low energies, and thus imaging at or below the secondary peak maximum is the normal imaging mode.

Hyperspectral imaging is accomplished by scanning either the photon energy, or the analysis energy, or both, over several spectral features of interest, and collecting a stack of images at a step size relevant to the problem. The resulting image stack may contain from 10's to 1000's of images. Even with fairly coarse step sizes, and poor counting statistics, good quality images can be extracted, and contrast mechanisms separated out. The left hand side of Fig. 8 shows part of a VPPEM image stack of a calcium/aluminum alloy after annealing [54]. The calcium/aluminum alloy is a distortion strengthened alloy that has potential in high conductivity self-supporting overhead electrical transmission lines. Overheating of the alloy causes the Ca and Al to react, and form a range of intermetallics [55].

The VPPEM detection energy used for the images of Fig. 8 was 1.0 eV, and thus the electron energy above the Fermi level is approximately 5.0 eV. Therefore, we can expect the information depth to be greater than 1-2 nm, and we are looking more at the bulk alloy, than the surface. The complete image stack was over two spectral ranges of photon energy. These ranges are 20-45 eV and 70-90eV covering the Ca 3p, and the Al 2p core levels with 1 eV step size. Normalized spectra from the complete image stack are shown on the right hand side of Fig. 8. These spectra are obtained iteratively from different areas in the image stack with the aim of isolating the most different spectra, the endpoint spectra. The two most different spectra were determined for the image stack, and these are shown as the red and blue spectra, the endpoint spectra E1 and E2 in Fig. 8. These spectra are treated as signals, not photoelectron spectra, and they are uncorrected for the beamline monochrometer function which has broad peaks at 30eV and 80 eV.

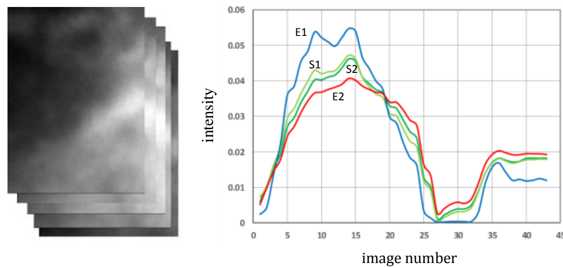

Fig 8 VPPEM hyperspectral image stack and endpoint spectra. Ref [54]

Difference images were created using the endpoint spectra that that measured the similarities of the images to the two end point spectra. This was accomplished by a root mean square (RMS) comparison of each individual pixel spectrum with the E1 and E2 spectra. The image intensities are a linear function of fitting error, light is a good fit to the spectra, and dark is a poor fit. Just the lower half of the spectra were used because of the difficulty of accurate image registration across the complete image stack.

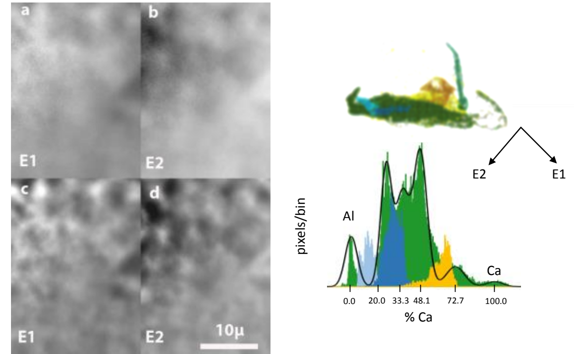

Fig. 9 Endpoint images and scatter diagram. On the left a) and b) endpoint images E1 and E2, c) and d) endpoint images after Lucy-Richardson deconvolution. On the right scatter diagram and histogram from images c) and d). Ref [54]

Fig. 9 shows the RMS endpoint images and scatter diagram. On the left a) and b) endpoint images E1 and E2. Images Fig. 9 c) and d) are the endpoint images after 50 iterations of the Lucy-Richardson deconvolution [56, 57] using the theoretical VPPEM point spread function [5]. We can create a scatter diagram from the deconvoluted endpoint images, and this is shown on the right of Fig 9. The images E and E2 are largely anticorrelated so that we can rotate the scatter diagram 45° in the plane of the diagram, and take a histogram across the long axis of the distribution. This histogram is shown below the scatter diagram.

The sample is very complex with at least nine different features in the field of view. By isolating smaller areas we can show that there are six distinct features that represent the Ca and Al with four intermetallics across the compositional phase diagram. These features can be isolated by dividing up the histogram, and Fig. 10 shows the VPPEM image derived from this histogram. The four different intermetallics, and the Ca and Al are shown as a six color false color image. While Fig. 10 shows the Al-Ca intermetallics, there are other features that are a consequence of the distortion processing of the alloys. These additional features include voids, and other alloy phases, probably with carbon and oxygen. Beamline U4A cannot reach these additional core levels so they are shown as black areas in Fig. 10.

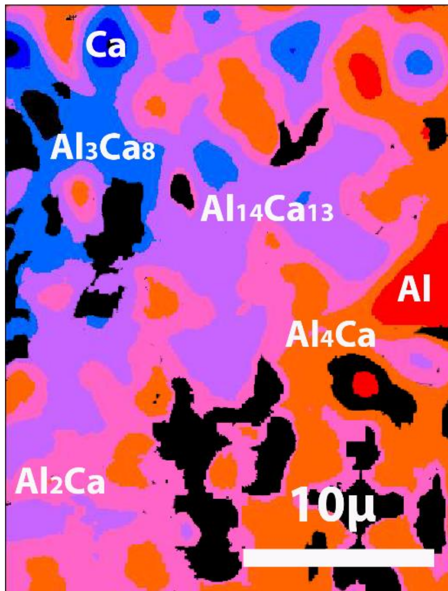

Fig. 10 Endpoint hyperspectral image of the reaction zones between Ca and Al. Ref [54]

The underlying point for our discussion here is that beamline U4A is a UV bending magnet source, and the photon flux was only 10^3-10^4 photons/sec/μ^2. This flux is very low for photoelectron microscopy, and yet highly detailed image data was recovered using hyperspectral image processing methods. With the current instrument using a 2 T field with 1.0 eV electrons, and 2 seconds per image, we can image down to 0.25 µ after Lucy-Richardson deconvolution.

This demonstrates that HAXPES hyperspectral imaging signal levels would very likely be sufficient to present information rich content, and could also be combined with LEEXPES in an image stack. Hyperspectral imaging is effective for the analysis of complex multiphase materials because the signal to noise in the image can be thought of as being due to the volume of the data compared to the noise. Thus the signal-to-noise in each independent signal axis is multiplicative, not additive [58].

Future Instrumentation

The current VPPEM is a prototype. Improvements can be made in both the instrumentation, and the data collection. The 2 T field can be increased to 20 T, the photon flux now available can be increased by six orders of magnitude, the photon range which is now 15-90 eV will be considerably extended from 100eV to 7.5 keV [59], the imaging energy can be decreased to 0.25 eV, and an order of magnitude more data can be collected. These improvements will take the spatial resolution into the low 10's of nanometers, and we will expect to combine LEEXPES and HX-VPPEM in the same data sets.

Conclusion

From these recent results from different photoelectron microscopes we can see that a new synthesis is possible. While many of the high energy microscopy experiments up to date have been proof of principle demonstrations, the basis for developing a new microscopy has been firmly established. We see it as important that LEEXPES, and HAXPES can be combined in one instrument. Such an instrument will collect a very wide range of spectroscopic information at one time, and the advantages of using hyperspectral methods, and data fusion then can be exploited.

With the technical basis for HAXPES imaging in place, what remains is to find the application driver for the technology to push it forward. Mesoscale analysis appears to be a natural fit, and there is a need for instrumentation in this area that can give detailed chemistry, and coordination in complex materials.

The several versions of hard x-ray microscope we have discussed here have different attributes. The direct high energy photoelectron HAXPEEM imaging approach promises the highest spatial resolution, possibly down to 10nm, but the HX-PEEM/VPPEM promises faster more convenient imaging with LEEXPES imaging providing higher resolution from image fusion. VPPEM imaging also promises analysis of 3D mesoscale structures with uneven features, and conductivities.

In summary, we can say that recent developments in instrumental and technique are opening up the world of photoelectron microscopy to include HAXPES, and we should see exciting advances in the near future.

References

[1] Crabtree, G.; Sarrao, J.; Alivisatos, P.; Barletta, W.; Bates, F.; Brown, G. French, R.; Greene, L.; Hemminger, J.; Kastner, M.et al. From Quanta to the Continuum: Opportunities for Mesoscale Science, 2012.
http://science.energy.gov/~/media/bes/pdf/reports/files/OFMS_rpt.pdf

[2] E. Bauer, Rep. Prog. Phys. 57, 895 (1994)

[3] E. Bauer, J. Electron Spectrosc. Relat. Phenom, **185**, 314 (2012)

[4] R. Browning, Rev. Sci. Instrum. **82**, 103703 (2011)

[5] R. Browning, Rev. Sci. Instrum. **85**, 033705 (2014)

[6] H. Mimura, S. Matsuyama, H. Yumoto, H. Hara, K. Yamamura, Y. Sano, M. Shibahara, K. Endo, Y. Mori, Y. Nishino, K. Tamasaku, M. Yabashi, T. Ishikawa, and K. Yamauchi, Jpn. J. Appli. Phys. **44** L539 (2005)

[7] M. Suzuki, N. Kawamura, M. Mizumaki, Y. Terada, T. Uruga, A. Fujiwara, H. Yamazaki, H. Yumoto, T. Koyama, Y. Senba, T. Takeuchi, H. Ohashi, N. Nariyama, K. Takeshita, H. Kimura, T. Matsushita, Y. Furukawa, T. Ohata, Y. Kondo J. Ariake, J. Richter, P. Fons, O. Sekizawa, N. Ishiguro, M. Tada, S. Goto, M. Yamamoto, M. Takata, and T. Ishikawa, Journal of Physics: Conference Series, **430**, 012017 (2013)

[8] Y. Terada, S. Homma-Takeda, A. Takeuchi, and Y. Suzuki, X-ray Optics. Instrum. **2010**, 317909 (2010)

[9] K. Horiba, Y. Nakamura, N. Nagamura, S. Toyoda, H. Kumigashira, M. Oshima, K. Amemiya, Y. Senba and H. Ohashi, Rev. Sci. Instrum. **82**, 113701 (2011)

[10] R. P. Winarski, M. V. Holt, V. Rose, P. Fuesz, D. Carbaugh, C. Benson, D. Shu, D. Kline, G. B. Stephenson, I. McNulty, and J. Maser, J. Synchrotron Radiat. **19**, 1056 (2012)

[11] C. J. Powell, and A. Jablonski, Nuc. Instum. Method. Phys. Res. **A601**, 54 (2009)

[12] M. P. Seah, Sur. Interface Anal. **44**, 497 (2012)

[13] Y. Hwu, W. L. Tsai, B. Lai, J. H. Je, G. H. Fecher, M. Bertolo, and G. Margaritondo, Surf. Sci. **480**, 188 (2001)

[14] H. Yasufuku, H. Yoshikawa, M. Kimura, K. Ito, K. Tani, S. Fukushima, Suf. Int. Analy, **36**, 892 (2004)

[15] T. Wakita, T. Taniuchi, K. Ono, M. Suzuki, N. Kawamura, M.i Takagaki, H. Miyagawa, F. Guo, T. Nakamura, T, Muro, H. Akinaga, and T. Yokoya, Jpn. J. Appl Phys. **45**, 1886 (2006)

[16] T. Taniuchi, T. Wakita, M. Takagaki, N. Kawamura, M. Suzuki, T. Nakamura, K. Kobayashi, M. Kotsugi, M. Oshima, H. Akinaga, H. Muraoka, and K. Ono, AIP Conference Proceedings **897**, 1353 (2007)

[17] T. Kinoshita, E. Ikenaga, J. Kim, S. Ueda, M. Kobata, J. R. Harries, K. Shimada, A. Ino, K. Tamasaku, Y. Nishino, T. Ishikawa, K. Kobayashi, W. Drube, and C. Kunz, Sur. Sci. **601**, 4754 (2007)

[18] M. Kotsugi, T. Wakita, T. Taniuchi, H. Maruyama, C. Mitsumata, K. Ono, M. Suzuki, N. Kawamura, N. Ishimatsu, M. Oshima, Y. Watanabe, and M. Taniguchi, IBM J. Res. & Dev. **55**, 13 (2011)

[19] C. Wiemann, M. Patt, S. Cramm, M. Escher, M. Merkel, A. Gloskovskii, S. Thiess, W. Drube, and C. M. Schneider, Appl. Phys. Lett. **100**, 223106 (2012)

[20] C.M. Schneider, C. Wiemann, M. Patt, V. Feyer, L. Plucinski, I.P. Krug, M. Escher, N. Weber, M. Merkel, O. Renault, and N. Barrett, J. Elec. Spectros. Relat. Phenom. **185**, 330 (2012)

[21] S. Tanuma, C. J. Powell, and D. R. Penn, Surf. Interface Anal. 43 689 (2011)

[22] T. Schmidt, A. Sala, H. Marchetto, E. Umbach, H. J. Freund, Ultramicroscopy **126**, 23 (2013)

[23] http://www.spring8.or.jp/pdf/en/ann_rep/98/P67-68.pdf

[24] Z. An, and Z. Shi, Optik **125**, 3150 (2014)

[25] R. A. Schowengerdt, Remote Sensing, Academic Press, Chap 8, 355 (2007)

[26] K. Artyushkova, J. O. Farrar, and J. E. Fulghum, Surf. Interface. Anal. **41**, 119 (2009)

[27] J. Sui, T. Adali, Q. Yu, and V. D. Calhoun, J. Neurosci. Methods, **204**, 68 (2012)

[28] R. Browning, J. Elec. Spectros. Relat. Phenom. **195**, 125 (2014)

[29] J. J. Quin, Phys. Rev. 126, 1453 (1962)

[30] D. R. Penn, Phys. Rev B **35**, 482 (1987)

[31] V. M. Silkin, E. V. Chulkov, and P. M. Echenique, Phys. Rev. B **68**, 205106 (2003)

[32] F. Offi, S. Iacobucci, L. Petaccia, S. Gorovikov, P. Vilmercati, A. Rizzo, A. Ruocco, A. Goldoni, G. Stefani, G. Panaccione, J. Phys. Condens. Matter **22**, 305002 (2010)

[33] H. Kanter Phys. Rev. B **1**, 522-536 (1970)

[34] V. P. Zhukov, E. V. Chulkov, P. M. Echenique, A. Marienfeld, M. Bauer, and M. Aeschlimann, Phys. Rev. B **76**, 193107 (7007)

[35] P. Jiricek, M. Cukr, I. Bartos, and J. Sadowski, Sur. Sci. **566-568**, 1196 (2004)

[36] A. Bauer, M. T. Cuberes, M. Prietsch, and G. Kaindl, J. Vac. Sci. Technol. B **11**, 1584 (1993)

[37] S. Hino, N. Sato, and H. Inokuchi, Chem. Phys. Lett. **37**, 494 (1976)

[38] F. Offi, S. Iacobucci, P. Vilmercati, A. Rizzo, A. Ruocco, A. Goldoni, M. Sacchi, G. Panaccione, Phys. Rev. B **77**, 201101 (2008)

[39] Y. Ozawa, Y. Nakayama, S. Machida, H. Kinjo, and H. Ishii, J. Elec. Spectros, Relat. Phenom. **197**, 17 (2014)

[40] G. K. L. Marx, P.-O. Jubert, A. Bischof, and R. Allenspach, Apppl. Phys. Let, **83**, 2925 (2003)

[41] K. Fedus, G. P. Karwasz, and Z. Idziaszek, Phys Rev. A **88**, 012704 (2013)

[42] S. A. Nepijko, N. N. Sedov, G. Schönhense, M. Escher, X. Bao, W. Huang, Ann. Phys. 2011, 9, 441.

[43] S. L. Christensen, B. m. Haines, U. D. Lanke, M. F. Paige, and S. G. Urquhart, IBM J. Res. Dev. **55**, 5 (2011)

[44] E. G. Kim, J. L. Brédas Organic Electronics **14**, 569-574 (2013)

[45] A. N. Buckley, A. J. Hartmann, R. N. Lamb, A. P. J. Stampfl, J. W. Freeland,
I. Coulthard, Surf. Interface Anal. **35**, 922-931 (2003)

[46] S. Tanuma, C. J. Powell, and D. R. Penn Surf. Interface Anal. **37**, 1-14 (2005)

[47] B. Ziaja, R. A. London, J. Hajdu J. Appl. Phys. **99**, 33514 (2006)

[48] M. P. Seah, I. S. Gilmore, Surf. Interface Anal. **31**, 835-846 (2001)

[49] S. Hajati, S. Tougaard, Anal Bioanal Chem **396**, 2741-2755 (2010)

[50] S. Oswald, R. Reiche, M. Zier, S. Baunack, K. Wetzig App. Sur. Sci. **252**, 3-10 (2005)

[51] S. Tougaard, J. of Elect. Spect. Relat. Phenom. **178**, 128-153 (2010)

[52] B. R. Strohmeier Surf. Interface Anal. **15,** 51-56 (1990)

[53] C.-I. Chang, Hyperspectral Data Processing: Algorithm Design and
Analysis, Chap. 11, Wiley, New York NY, 2013.

[54] R. Browning, Surf. Interface Anal. Published on-line DOI 10.1002/sia.5667 (2014)

[55] L. Tian, H. Kim, I. Anderson, A. M. Russell, Mat. Sci. Eng. A,
570, 106 (2013)

[56] L. B. Lucy, Astron. J. **79**, 745 (1974)

[57] W. H. Richardson, JOSA, **62**, 55 (1972)

[58] R. Browning, Surf. Interface Anal. 1993, 20, 495 (1993).

[59] R. Reininger, J. C.Woicik, S. L. Hulbert, D. A. Fischer, Nucl. Instrum. Meth. Phys. Res. A, **649**, 49 (2011)